Shahnazian, Fatemeh; Adabi, Jafar; Pouresmaeil, Edris

# Frequency stability improvements based on automatic adjustment of synchronous power controller parameters

*Published in:*
Electrical Engineering

*DOI:*
10.1007/s00202-022-01558-9

Published: 01/10/2022

*Document Version*
Peer-reviewed accepted author manuscript, also known as Final accepted manuscript or Post-print

*Please cite the original version:*
Shahnazian, F., Adabi, J., & Pouresmaeil, E. (2022). Frequency stability improvements based on automatic adjustment of synchronous power controller parameters. *Electrical Engineering* , *104*(5), 3453-3463. https://doi.org/10.1007/s00202-022-01558-9

# Frequency Stability Improvements Based on Automatic Adjustment of Synchronous Power Controller Parameters

**Fatemeh Shahnazian[1], Jafar Adabi[1], Edris Pouresmaeil[2]**

[1] Department of Electrical and Computer Engineering, Babol (Noshirvani) University of Technology, Babol, Iran
[2] Department of Electrical Engineering and Automation, Alto University, Espoo, Finland

## Correspondence

Jafar Adabi, Babol (Noshirvani) University of Technology, Babol, Iran
Email: j.adabi@nit.ac.ir

## Abstract

This paper presents an automatic parameter adjustment technique for synchronous power controllers (SPC) in order to improve the dynamic frequency stability of the low inertia power systems. The proposed control method is based on a novel transfer function in which various grid and converter controller parameters involved in the stability studies have been thoroughly included. As the main contribution of this paper, the eigenvalue trajectory of the proposed transfer function has been determined, considering the variations of both virtual inertia and damping control parameters simultaneously. Furthermore, any corresponding operating point on this eigenvalue trajectory can be specified based on the desired frequency response characteristics of the system. Therefore, the inertia and damping coefficients of the converter controller can be simultaneously adjusted through the proposed controller algorithm as the second contribution of this paper. Also, as another novelty of this paper, it is demonstrated through analytical and theoretical studies that both damping ratio and natural frequency characteristics of a dynamic frequency response have profound effects on the controller parameter value adjustments. Simulation results have been employed in MATLAB/Simulink to confirm the performance of the proposed controller regarding the appropriate parameter value adjustments, development of the desired dynamic frequency responses, and the prominent interactions between the frequency response characteristics and the converter controller parameters.

**Keywords**: Frequency control, Renewable energy sources (RESs), Stability improvement, Synchronous power controller (SPC), Virtual inertia

## 1. Introduction

Currently, the overall layout of the electrical network is profoundly evolving from a synchronous generator (SG) dominant configuration into a converter dominant structure [1]. In fact, the global energy crisis, market issues, environmental costs, and the need for clean energy sources has made it inevitable to integrate the renewable energy sources (RESs) to the power grid. Therefore, various kinds of the RES topologies such as wind, photovoltaic, wave, etc. have been widely installed within the power grid in the past few years [2]. This rapid penetration of RESs leads to an increased share of converter-based energy sources compared to the available synchronous power suppliers of the grid. Thus, this modern configuration of the power system demands a novel properly designed controller which can guarantee the appropriate operation and the stability of the system while maximizing the hosting capacity of the grid [3,4].

The main drawback of this modern renewable-based configuration is that the integration of these non-synchronous generation units widely affects the angular frequency stability of the power networks since the interactive converters utilized in this structure are unable to provide frequency support characteristics, unlike the SGs [5,6]. Therefore, novel controller architectures are required in order to overcome this challenge as the integration of power electronics increases in the power system [7-9]. Conventionally, the power system stabilizers (PSS) have been used to damp the electro-mechanical (EM) oscillations of the system. However, the sporadic tuning feature of the PSS shows weakness against the changing operating conditions of the network and thus, leads to deterioration in system performance [10]. In this regard, additional RESs are required to provide frequency support through their converter interfaces [11].

To this end, several solutions have been proposed regarding the frequency stability issues and the desired inertial responses of the modern power systems [12-15]. Initially, droop control structures have been proposed to approximate the EM behavior of SGs in providing the

intended frequency support for the system [16]. Unfortunately, these traditional droop-based schemes are mostly effective for steady-state regulations of frequency while the dynamic states are neglected [17]. On the other hand, various studies propose detailed emulations of SG characteristics in the converter control structure [18]. Despite representing similar behavior to SGs, these models tend to add unnecessary complexity and computational burdens to the controller [13,19]. In this regard, other topologies have been employed based on the swing equation principles in order to provide the desired frequency support characteristics [20,21]. Among them, synchronous power controller (SPC) has been considered as a popular topology towards virtual inertia implementation in the electricity networks [22]. The overall structure of SPC consists of the cascaded voltage and current control loops through the usage of a virtual admittance [23]. Furthermore, a second order model can be utilized instead of the swing equation in this structure to provide an over-damped response for inertia emulation [22,24]. The inherent synchronism capability as well as over-current protection are considered as the superiorities of this method; however, tuning the control parameters can become complex here due to the nested loop structure [13].

In this regard, the appropriate adjustment of the control parameter values is of great importance in ensuring the sustainable performance of the system. Reference [25] proposes an optimization procedure to properly tune controller parameters and optimize the placement of the converter which can be considered scalable and efficient to some extent but still adds to the computational burdens of the controller. Recently, novel procedures such as model predictive control [26] and artificial intelligence approaches [27,28] have also been applied in the literature in order to determine the optimal operating point of the controller. On the other hand, the presence of these various control parameters necessitates detailed analytical studies on the interactions between controller components and the power loop sustainability and dynamics [29]. In this regard, several studies employ root-locus analysis as a powerful approach towards the evaluation of controller parameter impacts on dynamic performance of the system [30-32]. Among relevant literature, [33] demonstrates the profound effects of damping ratio on the transient response of the controller while considering this as the main determinative component influencing dynamic stability alongside virtual inertia.

This paper presents a novel control strategy which enables dynamic frequency stability improvements of the low inertia power grids through automatic adjustment of the SPC parameters. It is good to mention that the SPC method proposed by Rodriguez et al. in [34] has been utilized here as the basic control structure in order to develop the proposed control algorithm. In this regard, a novel transfer function is proposed which includes all the significant grid and converter controller parameters that should be involved in the stability studies. This comprehensive transfer function then provides the eigenvalue trajectory of the system based on the simultaneous variations of both virtual inertia and damping control parameters, which is considered as the first novelty of this paper. Since any specific operating point on this eigenvalue trajectory corresponds to a particular frequency response characteristic, a novel control algorithm has been designed to accurately adjust the controller parameter values based on the desired frequency response characteristics of the system, which is considered as the second contribution of this paper. Furthermore, analytical and theoretical studies have been performed to investigate the interactions between both damping ratio and natural frequency characteristics of a dynamic frequency response and the corresponding controller parameter values, as the third novelty of this paper. Finally, simulation results are provided in MATLAB/Simulink in order to demonstrate the functionality of the proposed controller in assigning proper controller parameter values to achieve the anticipated dynamic frequency responses as well as the major role of both damping ratio and natural frequency characteristics in the adjustment of converter controller parameters.

The rest of the paper is organized as follows. Section 2 outlines a general overview of the SPC structure, which is then followed by the provided mathematical equations and analytical studies in order to obtain a novel transfer function for the proposed controller. Section 3 provides a description of the system performance based on the proposed transfer function and studies the interactions between the intended frequency response characteristics and the converter controller parameters. The overall configuration of the proposed control algorithm is demonstrated in Sect. 4 while the simulation scenarios, as well as the results' discussions, are represented in Sect. 5. Finally, conclusions are specified in Sect. 6.

## 2. SPC-based Renewable Structures

Control of a grid-connected voltage source converter (VSC) utilized in a distributed generation (DG) unit can be obtained based on the SPC structure proposed in [34]. The general schematic diagram of this control method is demonstrated in Fig. 1. The SPC method consists of multiple control layers including the active and reactive power controller, the virtual admittance concept, and the current controller. As demonstrated in Fig. 1, the voltage reference $e^*$ is constructed based on the provided

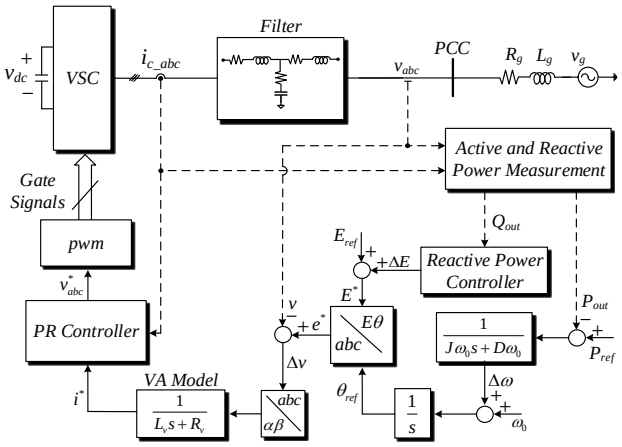


**Fig. 1.** General schematic diagram of the synchronous power controller

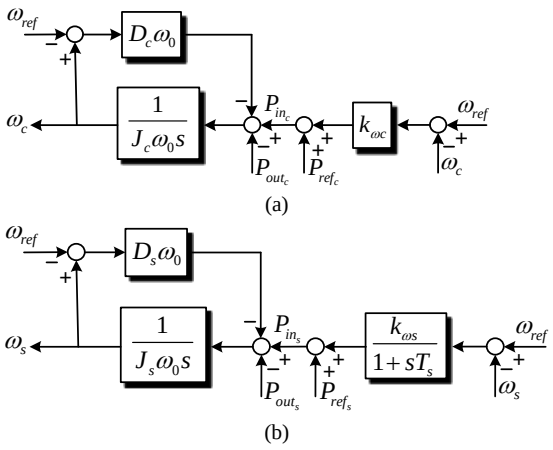


**Fig. 2.** Dynamic models of the electro-mechanical equations implemented in the: (a)VSC controller, and (b)SG-based grid

reference magnitude $E^*$ and the phase angle $\theta_{ref}$ . In this regard, $E^*$ can be produced by the reactive power controller while the EM equation of a synchronous machine is employed as the active power controller in order to create $\theta_{ref}$ . This structure results in an inherent synchronization capability which leads to a smooth transition between isolated and grid connected operation modes. In addition to that, the virtual admittance concept is also utilized in SPC in order to adjust the reference current provided for the current controller.

Focusing on the inertia emulation capabilities of SPC, Fig. 2a demonstrates the implementation of the EM model of a SG in the VSC controller. On the other hand, power grid operates mostly based on SG units. In this regard, the EM equations of the SG-based grid have been depicted in Fig. 2b.

It should be noted that while including the governor delay characteristics are inevitable in a SG structure, they can be easily omitted from the VSC controller. Therefore, the equations describing these two control structures can be written as:

$$P_{ref_c} - P_{out_c} - K_{\omega c}\left(\omega_c - \omega_{ref}\right) - D_c\omega_0\left(\omega_c - \omega_{ref}\right) = J_c\omega_0 s\left(\omega_c - \omega_{ref}\right) \quad (1)$$

$$P_{ref_s} - P_{out_s} - \frac{K_{\omega s}}{1+sT_s}\left(\omega_s - \omega_{ref}\right) - D_s\omega_0\left(\omega_s - \omega_{ref}\right) = J_s\omega_0 s\left(\omega_s - \omega_{ref}\right) \quad (2)$$

where, $\omega_{ref}$ , $\omega_0$ , and $\omega$ represent the reference, nominal, and output frequencies in rad/s while the subscripts $c$ and $s$ are utilized in order to distinguish between the converter and SG controller parameters. In addition to that, $J$ , $D$ , $K_\omega$ , and $T_s$ represent the characteristics of inertia, damping, droop, and the SG governor time constant respectively while $P_{ref}$ and $P_{out}$ demonstrate the reference and output active powers. In this regard, considering:

$$\Delta\omega_c = \omega_c - \omega_{ref} \quad (3)$$

$$\Delta P_c = P_{ref_c} - P_{out_c} \quad (4)$$

$$\Delta\omega_s = \omega_s - \omega_{ref} \quad (5)$$

$$\Delta P_s = P_{ref_s} - P_{out_s} \quad (6)$$

The transfer functions of the abovementioned controllers can be obtained as:

$$G_c(s) = \frac{\Delta\omega_c}{\Delta P_c} = \frac{1}{J_c\omega_0 s + D_c\omega_0 + K_{\omega c}} \quad (7)$$

$$G_s(s) = \frac{\Delta\omega_s}{\Delta P_s} = \frac{1}{J_s\omega_0 s + D_s\omega_0 + \frac{K_{\omega s}}{1+sT_s}} \quad (8)$$

On the other hand, a simplified equivalent schematic diagram of the grid connected VSC has been shown in Fig. 3. In order to study the stable operation of this system, it is good to keep in mind that load active power dynamics will eventually result in frequency dynamics. Since the SPC structure used in the converter controller is considered to be responsible for this frequency dynamic adjustment, the transfer function from $\Delta\omega_c$ to $\Delta P_l$ , denoted as $G(s)$ , would be one of the most beneficial functions used in our stability studies.

$$G(s) = \frac{\Delta\omega_c}{\Delta P_l} = \frac{\Delta\omega_c}{\Delta P_c} \times \frac{\Delta P_c}{\Delta P_l} = G_c(s) \times \frac{\Delta P_c}{\Delta P_l} \quad (9)$$

Considering a total impedance of $\vec{Z} = Z_c\angle\varphi$ between the converter internal voltage ( $\vec{E} = E_c\angle\delta_c$ ) and the grid voltage at PCC ( $\vec{V} = V_{PCC}\angle\delta_{PCC}$ ), the active power exchange can be calculated as:

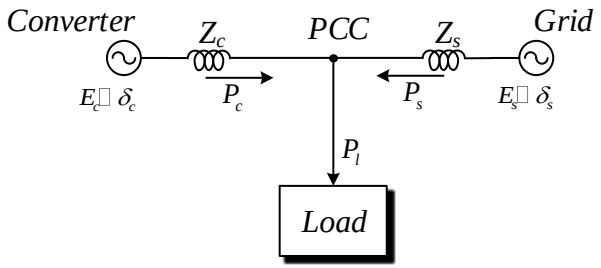


**Fig. 3.** Simplified schematic diagram of the grid-connected VSC

$$P_c = \frac{E_c V_{pcc}}{Z_c}\cos(\varphi-\delta) - \frac{V_{PCC}^2}{Z_c}\cos\varphi \tag{10}$$

where $\delta = \delta_c - \delta_{PCC}$ . Therefore, assuming a mostly inductive characteristic for the output impedance along with a small value for $\delta$ , (10) can be rewritten as:

$$P_c = \frac{E_c V_{pcc}}{X_c}\delta = P_c^{'}\delta \tag{11}$$

where, $X_c$ represents the inductive component of $Z_c$ . In this regard, we have $\Delta P_c = P_c^{'}\Delta\delta_c$ .

On the other hand, considering $\Delta\delta_c - \Delta\delta_s = \int(\Delta\omega_c - \Delta\omega_s)dt$ , we have:

$$\Delta P_c = P_c^{'}\Delta\delta_c = P_c^{'}\left(\frac{(\Delta\omega_c - \Delta\omega_s)}{s} + \Delta\delta_s\right) \tag{12}$$

Since $P_c + P_s = P_l$ and $\Delta\delta_s = \frac{\Delta P_s}{P_s^{'}} = \frac{\Delta P_l - \Delta P_c}{P_s^{'}}$ , (12) can be rewritten as:

$$\Delta P_c = \frac{P_c^{'}(\Delta\omega_c - \Delta\omega_s)}{s} + \frac{P_c^{'}(\Delta P_l)}{P_s^{'}} - \frac{P_c^{'}(\Delta P_c)}{P_s^{'}} \tag{13}$$

which leads to:

$$\frac{1}{P_c^{'}}\Delta P_c = \frac{1}{s}\Delta\omega_c - \frac{1}{s}\Delta\omega_s + \frac{1}{P_s^{'}}\Delta P_s \tag{14}$$

Since $\Delta\omega_c = G_c(s)\Delta P_c$ and $\Delta\omega_s = G_s(s)\Delta P_s$ , (14) can be rewritten as:

$$\frac{1}{P_c^{'}}\Delta P_c - \frac{1}{s}G_c(s)\Delta P_c = \frac{1}{P_s^{'}}\Delta P_s - \frac{1}{s}G_s(s)\Delta P_s \tag{15}$$

which then leads to:

$$\frac{\Delta P_s}{\Delta P_c} = \frac{\frac{1}{P_c^{'}} - \frac{1}{s}G_c(s)}{\frac{1}{P_s^{'}} - \frac{1}{s}G_s(s)} \tag{16}$$

Considering (16), the transfer function of $G(s)$ described in (9) can be represented as follows:

$$G(s) = \frac{\Delta\omega_c}{\Delta P_l} = G_c(s)\times\frac{\Delta P_c}{\Delta P_c + \Delta P_s} = G_c(s)\times\frac{1}{1+\frac{\Delta P_s}{\Delta P_c}} = \frac{G_c(s)}{1+\frac{\frac{1}{P_c^{'}} - \frac{1}{s}G_c(s)}{\frac{1}{P_s^{'}} - \frac{1}{s}G_s(s)}} \tag{17}$$

Since having the transfer function in terms of detailed grid and converter controller parameters would provide a clearer view for our further stability studies (provided in the next section), a more extended version of $G(s)$ can be developed as $G(s) = \frac{num(s)}{den(s)}$ where:

$$num(s) = (J_s\omega_0 T_s)s^3 + (J_s\omega_0 + D_s\omega_0 T_s)s^2 + (D_s\omega_0 + K_{\omega s} - P_s^{'}T_s)s - P_s^{'} \tag{18}$$

$$\begin{aligned} den(s) = {} & \left[\left(\frac{P_c^{'}+P_s^{'}}{P_c^{'}}\right)(J_c J_s\omega_0^2 T_s)\right]s^4 \\ & + \left[\left(\frac{P_c^{'}+P_s^{'}}{P_c^{'}}\right)(J_c J_s\omega_0^2 + J_c D_s\omega_0^2 T_s + J_s D_c\omega_0^2 T_s + J_s\omega_0 T_s K_{\omega c})\right]s^3 \\ & + \left[\left(\frac{P_c^{'}+P_s^{'}}{P_c^{'}}\right)(J_c D_s\omega_0^2 + J_c\omega_0 K_{\omega s} + J_s D_c\omega_0^2 + D_s D_c\omega_0^2 T_s \right. \\ & \left. + J_s\omega_0 K_{\omega c} + D_s\omega_0 T_s K_{\omega c}) - P_s^{'}\omega_0 T_s(J_s + J_c)\right]s^2 \\ & + \left[\left(\frac{P_c^{'}+P_s^{'}}{P_c^{'}}\right)(D_s D_c\omega_0^2 + D_c\omega_0 K_{\omega s} + D_s\omega_0 K_{\omega c} + K_{\omega s}K_{\omega c}) \right. \\ & \left. - P_s^{'}\omega_0(J_s + J_c) - P_s^{'}\omega_0 T_s(D_s + D_c) - P_s^{'}T_s K_{\omega c}\right]s \\ & - \left[P_s^{'}\omega_0(D_s + D_c) + P_s^{'}(K_{\omega s} + K_{\omega c})\right] \end{aligned} \tag{19}$$

As can be seen, this specific function contains various grid and converter controller parameters and thus can be very beneficial for stability study purposes.

## 3. Small Signal Stability Studies Based on the Proposed Transfer Function of G(s)

Unlike conventional grid structures based on SGs with physical limitations, the values of the virtually emulated control parameters are adjustable in a converter dominant structure. In this regard, root locus analysis can be applied as a powerful method in order to clarify the frequency stability constraints based on the converter controller

parameters' variations. Since for stability studies, eigenvalue analysis is performed on the denominator of the proposed transfer function, the quadratic equation of den(s) represented in (19) will be studied hereafter.

In order to evaluate the frequency stability of the system based on the variations of the virtually emulated inertia and damping factors of the converter ( $J_c$ and $D_c$ ), the root locus analysis for (19) has been demonstrated in Fig. 4a considering the $\omega_0 = 100\pi$ rad/s, $P_s^{'} = 1MW$ , $T_s = 10s$ , $K_{\omega s} = 2\times10^5$ , $J_s = 50$ , $D_s = 0$ , $P_c^{'} = 300\,kW$ , $K_{\omega c} = 5\times10^3$ , $J_c = 3$, and variable $D_c$ . As it can be seen, each point on the modal trajectory of this quadratic equation represents an operating point of the controller with specific $J_c$ and $D_c$ values. Therefore, as the dominant roots of the operating points move further away towards the left of the imaginary axis, the controller is expected to provide a more stable frequency response as a result. In this regard, 3 different values of $D_c$ on the proposed eigenvalue trajectory have been considered and then, the corresponding time domain frequency responses of the system have been demonstrated in Fig. 4b. As expected before, increasing the damping factor of $D_c$ in the controller can result in a more damped frequency response since the dominant roots of the corresponding operating points are moving towards more stable areas on the root locus trajectory as well.

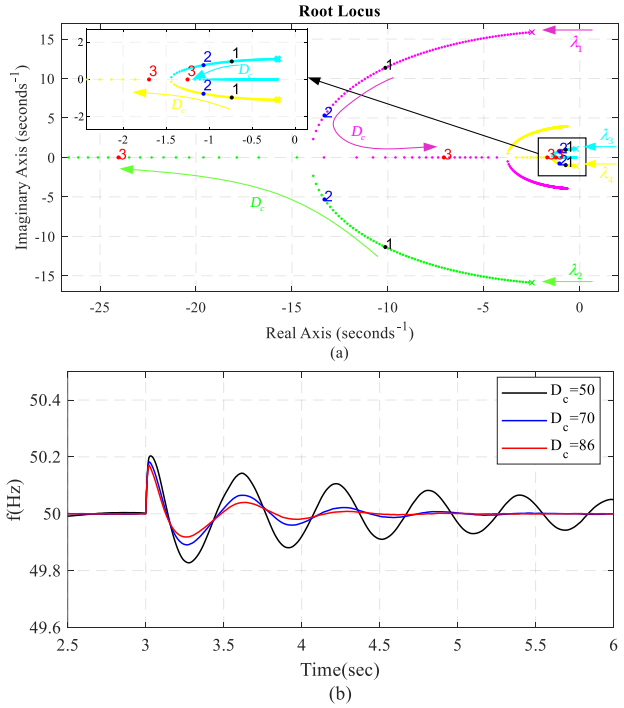


**Fig. 4.** The impacts of damping factor variations on the system: (a) eigenvalue trajectory, and (b) time domain frequency responses considering different D values

In addition to that, it is clear that each of the operating points with particular $J_c$ and $D_c$ values will eventually result in a dynamic frequency response with specific damping ratio ( $\xi$ ) and natural frequency ( $\omega_n$ ) characteristics. In this regard, the idea of an automatic parameter adjustment technique, using the eigenvalue trajectory of the proposed quadratic equation for the controller, will be thoroughly discussed in the next section. However, it would be beneficial to study the effects of $J_c$ and $D_c$ variations on both $\xi$ and $\omega_n$ characteristics in advance. For this purpose, Fig. 5a and Fig. 5b are provided here in order to demonstrate the influence of the controller parameter variations on $\xi$ and $\omega_n$ of the obtained frequency response, respectively.

As it can be seen in Fig. 5a, the damping ratio ( $\xi$ ) is not noticeably influenced by inertia variations while it considerably changes with damping factor ( $D_c$ ). At first, $\xi$ increases to the maximum of 1 as the damping factor increases and then gradually decreases to a minimum of about 0.6 and remains almost constant thereafter.

In this regard, it can be concluded that the intended damping ratio of a desired frequency response is able to suggest the appropriate ranges of $D_c$ to choose from. As mentioned above, one range of $D_c$ can be offered to provide $\xi < 0.6$ while, for greater amounts damping ratio, two ranges of $D_c$ will be suggested.

On the other hand, $D_c$ has only minor influence on $\omega_n$ (except in small values of $J_c$ ) as demonstrated in Fig. 5b. Thus, since $\omega_n$ clearly decreases when $J_c$ increases, the natural frequency of oscillation can be utilized in order to choose the proper inertia constant values. In this regard, the demand for a lower $\omega_n$ in frequency response could lead to a higher $J_c$ value selection.

Overall, it can be mentioned that based on the $\xi$ characteristics of the frequency response, acceptable ranges of $D_c$ are determined and then, based on the desired $\omega_n$ values, the corresponding $J_c$ can be specified among the available options. In addition to that, the lower intended $\omega_n$ values will lead to higher corresponding $J_c$ choices among the acceptable ranges of $D_c$ . The concepts of these relations between the proposed controller parameters and the system's dynamic frequency response characteristics will be utilized later in the simulation results analysis in order to validate the performance of the proposed controller.

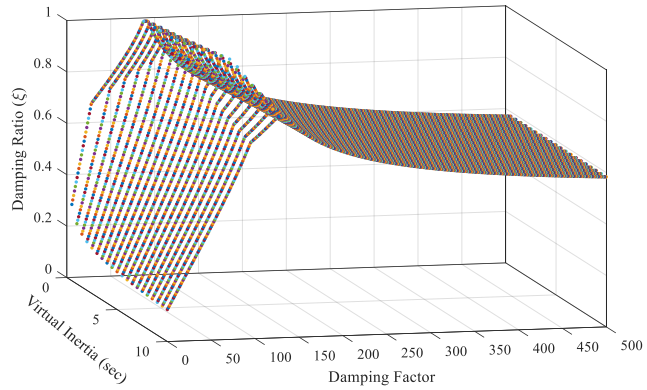


(a)

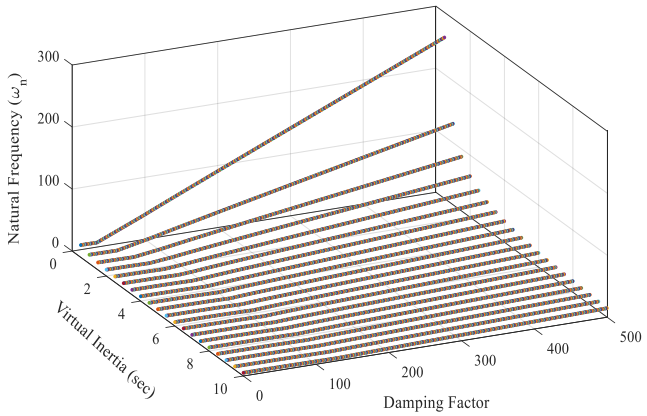


(b)

**Fig. 5.** The interactions between controller parameter values and frequency response characteristics: (a) influence of the controller parameter variations on damping ratio, and (b) influence of the controller parameter variations on natural frequency

## 4. Proposed Controller Design

As mentioned before, any specific operating point on the eigenvalue trajectory of the system will lead to a particular frequency response characteristic. Therefore, given the $\xi$ and $\omega_n$ characteristics of the intended dynamic frequency response, the corresponding controller parameters can be accurately determined based on the proposed root-locus analysis of the system. In this regard, the eigenvalue trajectory of the proposed transfer function of G(s) has been demonstrated in Fig. 6, where the variations of both control parameters of $J_c$ and $D_c$ have been considered at the same time. For this purpose, $J_c$ and $D_c$ have been varied from 0.5 to 10 and 0 to 500, respectively while, all other parameter values have been considered similar to those mentioned previously.

On the other hand, it should be noted that the both virtual components of inertia and damping utilized in the proposed converter control structure show considerable impact on the obtained frequency response dynamic. Thus, the ideal control method should be able to simultaneously adjust these two parameters in an automated procedure. Having that in mind, Fig. 7 presents the configuration of the proposed control algorithm in the form of a flow chart. As expected, the inertia and damping coefficients of the converter controller are automatically adjusted through the proposed controller algorithm, considering the desired dynamic frequency response characteristics. Most importantly, though, it should be mentioned that the main superiority of this method lies in the comprehensive transfer function of G(s), which has been proposed in order to thoroughly include the various system and controller parameters involved in the stability studies.

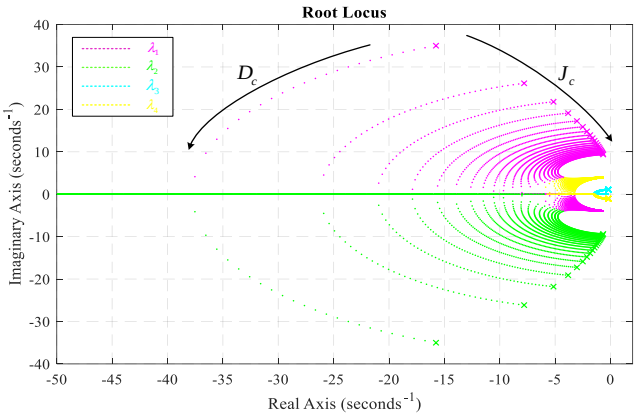


**Fig. 6.** Root locus trajectory of the proposed controller considering various inertia and damping coefficients

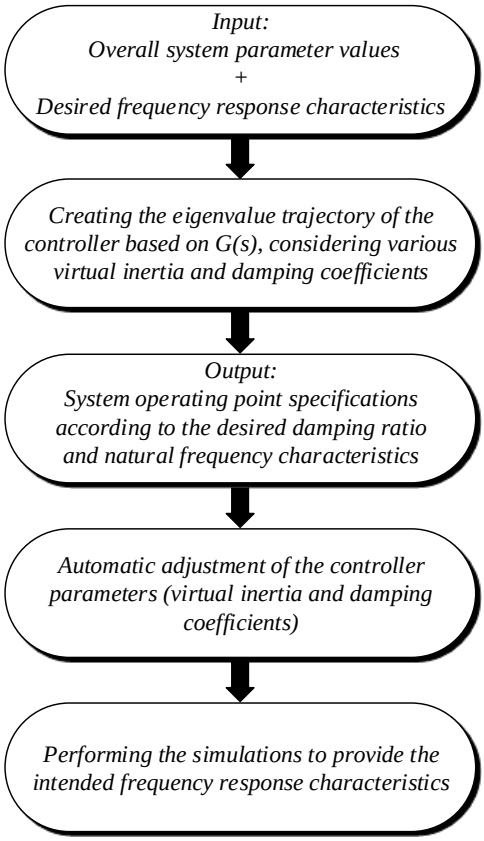


**Fig. 7.** Flow chart of the proposed controller algorithm for automatic adjustment of the SPC parameters

## 5. Simulation Results and Discussions

The overall configuration of the SPC-based grid-connected VSC, demonstrated in Fig. 8, has been simulated in MATLAB/Simulink. Moreover, the proposed controller described in Fig. 7 has also been applied to the abovementioned structure in order to validate the appropriate functionality of the algorithm through simulations. In this regard, the values of various circuit components as well as the operational conditions applied to the simulations are listed in Table 1.

In order to clarify more details about the above-mentioned system and the proposed controller, various aspects of the provided simulation scenarios have been studied separately in the following sections. In this regard, the overall performance of the SPC-based virtual synchronous generator (VSG) has been studied in Sect. 5.1 while, the appropriate operation of the proposed control algorithm has been modified in Sect. 5.2. In addition to that, the intended dynamic frequency responses of the system in accordance with the controller parameter specifications have been verified through simulations in Sect. 5.3.

### 5.1 Simulation Analysis of the SPC-based VSG

Considering the proposed configuration of the system and controller shown in Fig. 8, the grid-connected VSG is supposed to provide a share of load's active and reactive power requirements in accordance with the intended references. In this regard, the primitive references of the converter's active and reactive power ( $P_{refc1}$ and $Q_{refc1}$ ) are considered to be 200 KW and 20 KVar, respectively. Figure 9 shows load, converter, and grid's active and reactive power dynamics before and after the connection of the second load at 3s. As it can be seen, before 3s, the converter can perfectly provide $P_{refc1}$ and $Q_{refc1}$ while the remaining share of load's active and reactive power has been compensated by the grid. The same applies when after 3s, the second load is connected, and the active and reactive power requirements of the load are increased by fifty percent. In this regard, $P_{refc2}$ and $Q_{refc2}$ have been adjusted to 300 KW and 30 KVar, respectively and the controller follows the intended references after 3s, as well.

In addition to that, the SPC structure considered in this configuration includes the virtual inertia emulation characteristics which can improve the dynamic frequency responses of the converter. It should be mentioned that all simulation results in this paper are represented according to load dynamics at t=3s in order to keep the focus on the effects of the proposed inertia controller on frequency dynamics. In this regard, Fig. 10 shows the frequency dynamics of the SPC which have been developed as a result of the load dynamics at 3s. As it can be seen, the controller can provide the desired stability of the frequency response, integrating the inertia characteristics into the conventional converter control structure.

Overall, the abovementioned configuration is perfectly capable of providing the intended active and reactive power references, while the virtual inertia emulation characteristics of the SPC controller considered in this structure can make the desired SG-like dynamic frequency response available as well.

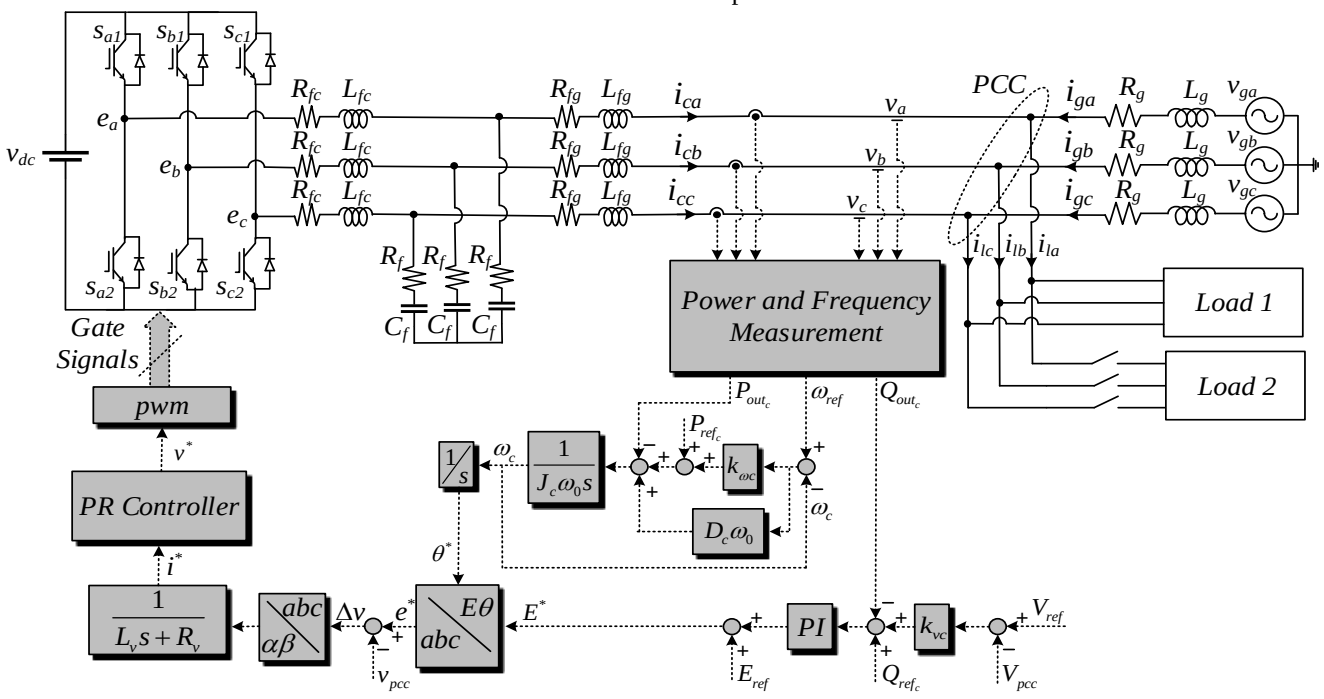


**Fig. 8.** Overall configuration of the simulated SPC-based VSC structure connected to the grid

**Table 1.** Parameter values and operational conditions applied to simulations

| Items | Values |
|---|---|
| dc-link voltage $v_{dc}$ | 1800 V |
| Grid voltage ($v_g$) (L-L,rms) | 400 V |
| Converter-side filter resistance ($R_{fc}$) | 0.4 Ω |
| Grid-side filter resistance ($R_{fg}$) | 0.3 Ω |
| Shunt filter resistance ($R_f$) | 5 Ω |
| Converter-side filter inductance ($L_{fc}$) | 2 mH |
| Grid-side filter inductance ($L_{fg}$) | 1 mH |
| Shunt filter capacitance ($C_f$) | 9 μF |
| Grid resistance ($R_g$) | 1 mΩ |
| Grid inductance ($L_g$) | 0.04 mH |
| Nominal frequency ($f_0$) | 50 Hz |
| Switching/Sampling frequency | 10 KHz |
| Frequency droop coefficient ($K_{\omega c}$) | 5000 |
| Voltage droop coefficient ($K_{vc}$) | 100 |
| Virtual resistance of the controller (load1 connected) ($R_{v1}$) | 1.39 Ω |
| Virtual inductance of the controller (load1 connected) ($L_{v1}$) | 0.4 mH |
| Virtual resistance of the controller (load2 connected) ($R_{v2}$) | 0.93 Ω |
| Virtual inductance of the controller (load2 connected) ($L_{v2}$) | 0.3 mH |
| Load1 active power ($P_{L1}$) | 300 KW |
| Load1 reactive power ($Q_{L1}$) | 30 KVar |
| Primitive reference of converter active power ($P_{refc1}$) | 200 KW |
| Primitive reference of converter reactive power ($Q_{refc1}$) | 20 KVar |

### 5.2 Simulation Verification of the Proposed Control Algorithm

In order to evaluate the appropriate performance of the proposed control algorithm, 3 different frequency response characteristics have been considered and the corresponding simulation results are provided here. As mentioned in the flowchart of Fig. 7, the proposed algorithm firstly creates the eigenvalue trajectory of the system based on the overall system parameter values while considering various amounts of virtual inertia and damping coefficients. Then in the next step, the appropriate operating points can be identified based on the desired $\xi$ and $\omega_n$ values.

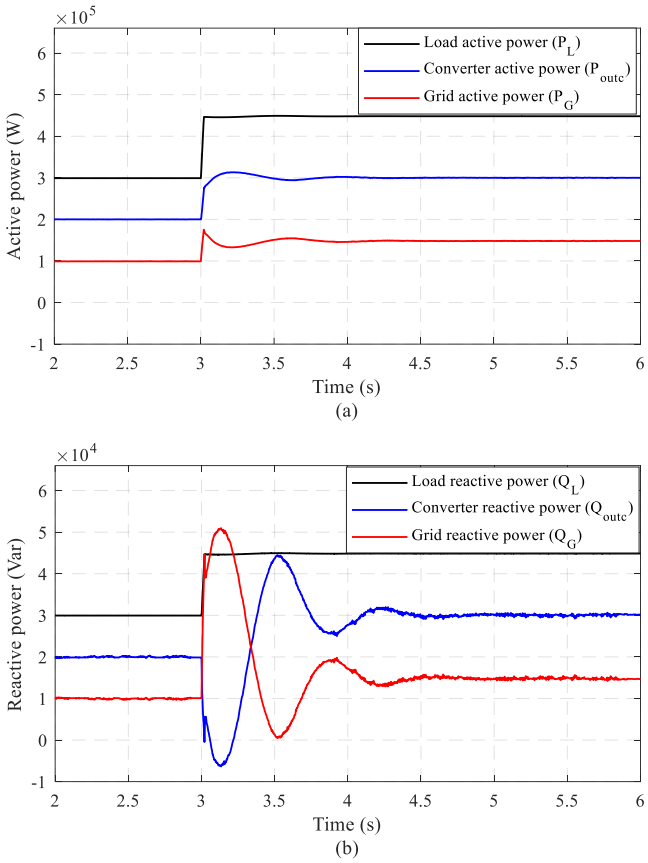


**Fig. 9.** Simulation results of the SPC-based structure considering second load connection at 3s: (a) load, converter, and grid's active power dynamics, and (b) load, converter, and grid's reactive power dynamics

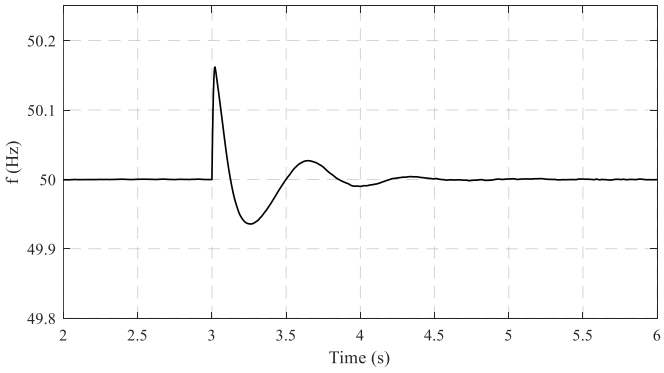


**Fig. 10.** Frequency dynamics of the proposed SPC-based controller considering load dynamics at 3s

Finally, the algorithm will automatically adjust the virtual inertia and damping coefficients of the SPC controller, shown in Fig. 8. With that in mind, Fig. 11a demonstrates the eigenvalue trajectory of the simulated configuration as well as the convenient operating points of the system, considering the desired frequency response characteristics. These identified parameter values have then been applied to the controller and the obtained simulation results are demonstrated in Fig. 11b.

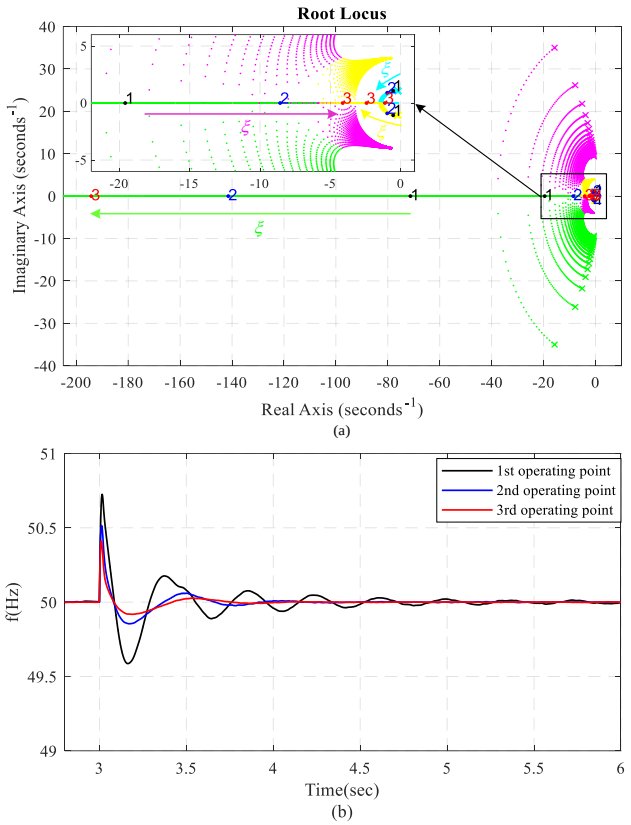


**Fig. 11.** Simulation results of the proposed control algorithm considering 3 different frequency response characteristics: (a) demonstration of the corresponding operating points detected on the eigenvalue trajectory, and (b) time domain frequency responses of the system regarding the adjusted operating points.

As it can be seen in Fig. 11a, three different frequency response characteristics considering $\xi$ values of 0.72, 0.86, and 1 have been selected while the $\omega_n$ values have also been set to 23.3, 38.2, and 50.5 respectively. In this regard, as the intended operating points are moving further away towards the left of the imaginary axis in the root-locus trajectory, the simulation results show more stability in the time domain frequency responses of the system. Furthermore, Fig. 11b shows that the overshoot decreases while $\xi$ increases and the frequency response becomes more stable as expected. Therefore, the proposed control algorithm is perfectly capable of the appropriate adjustment of controller parameters in accordance with the desired frequency response dynamics.

### 5.3 Simulation Analysis of the Correlations Between Controller Parameters and the Dynamic Frequency Response of the System

As mentioned before, both $\xi$ and $\omega_n$ characteristics are dominant and effective in determining the controller parameter values. This can be clearly acknowledged in Fig. 11b where the second operating point with $\xi$=0.7 still leads to a few fluctuations in frequency before reaching the steady-state, whereas a more smooth interaction between VSG and the power grid is expected with this damping ratio [35]. The reason for this is that the effect of the natural oscillation frequency ($\omega_n$) has been neglected here, while both $\xi$ and $\omega_n$ parameters should be carefully considered in dynamic frequency studies.

In order to evaluate the correlations between these frequency response characteristics and the adjusted controller parameter values, two operating points are selected considering $\xi$=0.7 and different $\omega_n$ values. Meanwhile, it is expected that with the same amount of damping ratio, a decrease in $\omega_n$ will lead to a decrease in dynamic frequency response oscillations. In this regard, as demonstrated in Fig. 5a, considering $\xi$>0.6 suggests two ranges of $D_c$ for the controller among which, as mentioned in Fig. 5b, the need for a lower $\omega_n$ value leads to the selection of the $D_c$ range corresponding to the larger inertia coefficients. Therefore, decreasing $\omega_n$ from 23.3 to 7 while maintaining $\xi$=0.7 results in the two operating points of $\begin{cases} J_c = 0.5 \\ D_c = 30 \end{cases}$ and $\begin{cases} J_c = 10 \\ D_c = 216 \end{cases}$, respectively. Figure 12 demonstrates the dynamic frequency response of the proposed system, considering the above-mentioned operating points. It is clearly shown that the adjustment of virtual inertia and damping coefficients with the aim of reducing $\omega_n$ will lead to a more damped frequency response as expected.

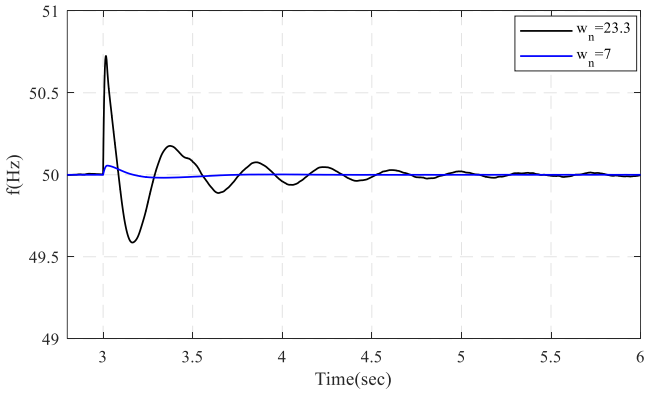


**Fig. 12.** Frequency dynamics of the proposed control algorithm considering two different frequency response characteristics

## 5. Conclusion

This paper presented an automatic parameter adjustment method for SPCs to enhance the dynamic frequency stability of the low inertia grids. In this regard, a novel transfer function has been proposed in terms of detailed grid and converter controller parameters which are involved in the stability studies. Then, considering the simultaneous variations of both virtual inertia and damping parameters of the controller, the eigenvalue trajectory has been determined for the denominator of this proposed transfer function as the first contribution of this paper. Furthermore, since any specific operating point on this eigenvalue trajectory of the system leads to a particular frequency response characteristic, a novel control algorithm has been proposed as the second contribution of this paper which can accurately adjust controller parameter values according to the desired frequency response characteristics of the system. Finally, analytical and theoretical studies have demonstrated profound interactions between both damping ratio and natural frequency characteristics of dynamic frequency response and the corresponding controller parameter values, as another novelty of this paper. Simulation results in MATLAB/Simulink have demonstrated the proficiency of the proposed controller in assigning appropriate controller parameter values in order to obtain the intended dynamic frequency responses as well as the significant role of both $\xi$ and $\omega_n$ characteristics in the stability studies.


## Funding

This work was supported by the Babol Noshirvani University of Technology under Grant BNUT/389051/99.


## Conflicts of interest

The authors have no conflict of interest to declare.

## References


1. IEA (2020), World Energy Outlook 2020, IEA, Paris https://www.iea.org/reports/world-energy-outlook-2020.

2. Phurailatpam C, Rather ZH, Bahrani B, Doolla S (2020) Measurement-Based Estimation of Inertia in AC Microgrids. IEEE Transactions on Sustainable Energy 11 (3):1975-1984. doi:10.1109/TSTE.2019.2948224

3. Santos SF, Fitiwi DZ, Shafie-Khah M, Bizuayehu AW, Cabrita CMP, Catalão JPS (2017) New Multistage and Stochastic Mathematical Model for Maximizing RES Hosting Capacity—Part I: Problem Formulation. IEEE Transactions on Sustainable Energy 8 (1):304-319. doi:10.1109/TSTE.2016.2598400

4. Santos SF, Fitiwi DZ, Shafie-khah M, Bizuayehu AW, Cabrita CMP, Catalão JPS (2017) New Multi-Stage and Stochastic Mathematical Model for Maximizing RES Hosting Capacity—Part II: Numerical Results. IEEE Transactions on Sustainable Energy 8 (1):320-330. doi:10.1109/TSTE.2016.2584122

5. Gu H, Yan R, Saha TK (2018) Minimum Synchronous Inertia Requirement of Renewable Power Systems. IEEE Transactions on Power Systems 33 (2):1533-1543. doi:10.1109/TPWRS.2017.2720621

6. Shahnazian F, Adabi J, Pouresmaeil E, Mehrasa M, Catalão JPS Circulating Current Elimination of Grid-Connected Modular Multilevel Converters. In: 2018 IEEE International Conference on Environment and Electrical Engineering and 2018 IEEE Industrial and Commercial Power Systems Europe (EEEIC / I&CPS Europe), 12-15 June 2018 2018. pp 1-6. doi:10.1109/EEEIC.2018.8494496

7. Chen T, Guo J, Chaudhuri B, Hui SY (2020) Virtual Inertia From Smart Loads. IEEE Transactions on Smart Grid 11 (5):4311-4320. doi:10.1109/TSG.2020.2988444

8. Kumar KA, Kushwaha P, Prakash V, Bhakar R, Tiwari H, Sharma KG Inertia Emulation Trends in Low Carbon Power System. In: 2019 8th International Conference on Power Systems (ICPS), 20-22 Dec. 2019 2019. pp 1-6. doi:10.1109/ICPS48983.2019.9067707

9. Saeedian M, Pournazarian B, Taheri S, Pouresmaeil E (2021) Provision of Synthetic Inertia Support for Converter-Dominated Weak Grids. IEEE Systems Journal:1-10. doi:10.1109/JSYST.2021.3060866

10. Padilla LAO, Gallardo RP, Saldaña JAM (2019) A Robustness Study of Power System Stabilizers using Dynamic Modeling. IEEE Latin America Transactions 17 (03):513-519. doi:10.1109/TLA.2019.8863322

11. Xiong L, Liu X, Zhang D, Liu Y (2021) Rapid Power Compensation-Based Frequency Response Strategy for Low-Inertia Power Systems. IEEE Journal of Emerging and Selected Topics in Power Electronics 9:4500-4513. doi: 10.1109/jestpe.2020.3032063

12. Saeedian M, Sangrody R, Shahparasti M, Taheri S, Pouresmaeil E (2021) Grid-Following DVI-Based Converter Operating in Weak Grids for Enhancing Frequency Stability. IEEE Transactions on Power Delivery:1-1. doi:10.1109/TPWRD.2021.3059898

13. Tamrakar U, Shrestha D, Maharjan M, Bhattarai BP, Hansen TM, Tonkoski R (2017) Virtual Inertia: Current Trends and Future Directions. Applied Sciences 7 (7). doi:10.3390/app7070654

14. Wu Y, Yang W, Hu Y, Dzung P (2019) Frequency Regulation at a Wind Farm Using Time-Varying Inertia and Droop Controls. IEEE Transactions on Industry Applications 55:213-224

15. Mahish P, Pradhan A (2020) Distributed Synchronized Control in Grid Integrated Wind Farms to Improve Primary Frequency Regulation. IEEE Transactions on Power Systems 35:362-373

16. Sun D, Liu H, Gao S, Wu L, Song P, Wang X (2020)

Comparison of Different Virtual Inertia Control Methods for Inverter-based Generators. Journal of Modern Power Systems and Clean Energy 8 (4):768-777. doi:10.35833/MPCE.2019.000330

17. Meng X, Liu J, Liu Z (2019) A Generalized Droop Control for Grid-Supporting Inverter Based on Comparison Between Traditional Droop Control and Virtual Synchronous Generator Control. IEEE Transactions on Power Electronics 34 (6):5416-5438. doi:10.1109/TPEL.2018.2868722

18. 4. Rosso R, Cassoli J, Buticchi G, Engelken S, Liserre M (2019) Robust Stability Analysis of LCL Filter Based Synchronverter Under Different Grid Conditions. IEEE Transactions on Power Electronics 34:5842-5853

19. Vetoshkin L, Müller Z A supervisory MPC for synchronverter. In: 2020 21st International Scientific Conference on Electric Power Engineering (EPE), 19-21 Oct. 2020 2020. pp 1-6. doi:10.1109/EPE51172.2020.9269232

20. Xu H, Yu C, Liu C, Wang Q, Zhang X (2020) An Improved Virtual Inertia Algorithm of Virtual Synchronous Generator. Journal of Modern Power Systems and Clean Energy 8 (2):377-386. doi:10.35833/MPCE.2018.000472

21. Zheng T, Chen L, Guo Y, Mei S (2018) Comprehensive control strategy of virtual synchronous generator under unbalanced voltage conditions. IET Generation, Transmission & Distribution 12 (7):1621-1630

22. Zhang W, Cantarellas AM, Rocabert J, Luna A, Rodriguez P (2016) Synchronous Power Controller With Flexible Droop Characteristics for Renewable Power Generation Systems. IEEE Transactions on Sustainable Energy 7 (4):1572-1582. doi:10.1109/TSTE.2016.2565059

23. Rodríguez P, Citro C, Candela JI, Rocabert J, Luna A (2018) Flexible Grid Connection and Islanding of SPC-Based PV Power Converters. IEEE Transactions on Industry Applications 54 (3):2690-2702. doi:10.1109/TIA.2018.2800683

24. Zhang W, Remon D, Mir A, Luna A, Rocabert J, Candela I, Rodriguez P Comparison of different power loop controllers for synchronous power controlled grid-interactive converters. In: 2015 IEEE Energy Conversion Congress and Exposition (ECCE), 20-24 Sept. 2015 2015. pp 3780-3787. doi:10.1109/ECCE.2015.7310194

25. Poolla BK, Groß D, Dörfler F (2019) Placement and Implementation of Grid-Forming and Grid-Following Virtual Inertia and Fast Frequency Response. IEEE Transactions on Power Systems 34 (4):3035-3046. doi:10.1109/TPWRS.2019.2892290

26. Ademola-Idowu A, Zhang B (2021) Frequency Stability Using MPC-Based Inverter Power Control in Low-Inertia Power Systems. IEEE Transactions on Power Systems 36 (2):1628-1637. doi:10.1109/TPWRS.2020.3019998

27. Baltas GN, Lai NB, Marin L, Tarrasó A, Rodriguez P (2020) Grid-Forming Power Converters Tuned Through Artificial Intelligence to Damp Subsynchronous Interactions in Electrical Grids. IEEE Access 8:93369-93379. doi:10.1109/ACCESS.2020.2995298

28. Yap KY, Sarimuthu CR, Lim JM (2020) Grid Integration of Solar Photovoltaic System Using Machine Learning-Based Virtual Inertia Synthetization in Synchronverter. IEEE Access 8:49961-49976. doi:10.1109/ACCESS.2020.2980187

29. Zhang W, Tarraso A, Rocabert J, Luna A, Candela JI, Rodriguez P (2019) Frequency Support Properties of the Synchronous Power Control for Grid-Connected Converters. IEEE Transactions on Industry Applications 55 (5):5178-5189. doi:10.1109/TIA.2019.2928517

30. Shahnazian F, Adabi J, Pouresmaeil E (2021) Enhanced control of voltage source converters considering virtual inertia theory. International Transactions on Electrical Energy Systems. doi: 10.1002/2050-7038.13245

31. Khazaei J, Tu Z, Liu W (2020) Small-Signal Modeling and Analysis of Virtual Inertia-Based PV Systems. IEEE Transactions on Energy Conversion 35 (2):1129-1138. doi:10.1109/TEC.2020.2973102

32. Marin L, Tarras´ A, Candela I, Rodriguez P Stability Analysis of a Grid-Connected VSC Controlled by SPC. In: 2018 7th International Conference on Renewable Energy Research and Applications (ICRERA), 14-17 Oct. 2018 2018. pp 1209-1214. doi:10.1109/ICRERA.2018.8567018

33. Zhang W, Remon D, Rodriguez P (2017) Frequency support characteristics of grid-interactive power converters based on the synchronous power controller. IET Renewable Power Generation 11 (4):470-479. doi:https://doi.org/10.1049/iet-rpg.2016.0557

34. Rodriguez P, Candela I, Luna A Control of PV generation systems using the synchronous power controller. In: 2013 IEEE Energy Conversion Congress and Exposition, 15-19 Sept. 2013 2013. pp 993-998. doi:10.1109/ECCE.2013.6646811

35. Abdollahi M, Candela JI, Rocabert J, Aguilar RSM, Hermoso JR Synchronous power controller merits for dynamic stability improvement in long line by renewables. In: 2016 IEEE International Conference on Renewable Energy Research and Applications (ICRERA), 20-23 Nov. 2016 2016. pp 760-765. doi:10.1109/ICRERA.2016.7884438